J Mater Sci: Mater Med (2009) 20:2105–2116
DOI 10.1007/s10856-009-3780-7

Human aortic endothelial cell response to 316L stainless steel material microstructure

Animesh Choubey · Denes Marton · Eugene A. Sprague

Received: 3 February 2009 / Accepted: 7 May 2009 / Published online: 23 May 2009

Abstract The role of metal microstructure (e.g. grain sizes) in modulating cell adherence behavior is not well understood. This study investigates the effect of varying grain sizes of 316L stainless steel (SS) on the attachment and spreading of human aortic endothelial cells (HAECs). Four different grain size samples; from 16 to 66 μm (ASTM 9.0-4.9) were sectioned from sheets. Grain structure was revealed by polishing and etching with glycergia. Contact angle measurement was done to assess the hydrophilicity of the specimens. Atomic force microscopy (AFM) and X-ray photoelectron spectroscopy (XPS) were used to characterize the roughness and surface chemistry of the specimens. Cells were seeded on mechanically polished and chemically etched specimens followed by identification of activated focal adhesion sites using fluorescently tagged anti-pFAK (phosphorylated focal adhesion kinase). The 16 μm grain size etched specimens had significantly ($P < 0.01$) higher number of cells attached per cm^2 than other specimens, which may be attributed to the greater grain boundary area and associated higher surface free energy. This study shows that the underlying material microstructure may influence the HAEC behavior and may have important implications in endothelialization.

A. Choubey
Department of Biomedical Engineering, University of Texas at San Antonio, One UTSA Circle, San Antonio, TX 78249-1644, USA

A. Choubey (✉) · D. Marton · E. A. Sprague
Departments of Radiology and Biomedical Engineering, University of Texas Health Science Center at San Antonio, 7703 Floyd Curl Drive, San Antonio, TX 78229-3900, USA
e-mail: animesh.choubey@gmail.com

1 Introduction

A distinguishing quality of metals as vascular implants is their ability to be colonized by endothelial cells (EC). Any improvement in metal-EC interaction translates into better healing of implants [1–4]. Previous studies [5–8] have suggested that rough surfaces may provide for faster stent endothelialization. Some studies [6, 7] have demonstrated that endothelial cells could "sense" surface topography at the micrometer (μm) scale. Palmaz et al. [6] observed that surface discontinuities at microscopic scale influence the conformation and motion dynamics of migrating endothelial cells. They also investigated the effect of defined surface features on endothelial cell migration speed, long axis orientation, shape, size and density and concluded that the endothelial cell migration rates significantly increased (up to 64%) on surfaces with grooves ranging from 3 to 22 μm compared to the flat control surfaces. Endothelial cells had a more elongated shape on grooved surfaces, as a consequence of increased migration rate. This work was confirmed in a more recent study [7] in which stents with microscopic parallel grooves were placed in carotid arteries of pigs. The authors of this study reported that at 1 week after implantation, stents with grooved surfaces exhibited an endothelialization rate almost double that observed on stents with smooth surfaces. Rapid stent endothelialization has been shown to reduce in-stent thrombus and obstruction due to intimal thickening [9, 10]. Furthermore, delayed endothelialization has been associated with late adverse events among patients treated with different antiproliferative therapies [11, 12].

Recently, Dibra et al. [13] conducted the first clinical study to evaluate the relationship between stent surface topography and outcome in patients undergoing implantation of electrochemically polished and sand blasted stent

surfaces. They observed that both types of stents were equivalent with respect to late lumen loss but the observed difference indicated a reduced restenosis for the sand blasted stent surface as compared to smooth electrochemically polished stents.

Various other surface modification techniques for enhancing the rate of endothelialization have been investigated [14–19] and the effect of material surface morphology on cell (osteoblast, fibroblasts, endothelial cells) adhesion, spreading, proliferation and protein adsorption has been extensively studied experimentally and theoretically [20–24]. However, the focus of all these investigations has been on surfaces with artificially created regular surface morphology (micro or nano patterning using different techniques), and have not addressed how inherent random material microstructure features affect the human aortic endothelial cell behavior. The influence of the surface microstructure is dominant during the early stages of the biological response; however it is also known that the very first biochemical interactions at an implant site are decisive with respect to the course of later reactions and the final tissue architecture at the interface [25–28]. To the best of our knowledge no study has been done to investigate the effect of varying inherent material microstructure (grain size) on endothelial cells. Therefore, this study aims at understanding the response of endothelial cells to 316L SS microstructure. Specifically, this study examines the influence of 316L SS grain size and grain boundary exposure on HAEC adhesion and morphology. Contact angle, optical and atomic force microscopy (AFM) and X-ray photoelectron spectroscopy (XPS) have been used to characterize these surfaces. Fluorescence microscopy was performed to analyze the HAEC density, spreading area and number of activated focal adhesion sites formed on samples of different grain sizes.

2 Materials and methods

2.1 Mechanical polishing

Mechanical polishing of samples was performed following ASTM E3-95 standard [29] for preparation of metallographic specimens. **S**amples of four different grain sizes (16, 31, 47 and 66 μm) were cut into 1 × 1 cm squares from cold worked 316L SS (Fort Wayne Metals, IN) material. These cut samples were cold mounted in a mixture of epoxy resin and hardener (5:1) (Buehler, Lake Bluff, IL) for 8 h. After cold mounting the samples were polished in order to remove coarse scratches and deformations utilizing a series of decreasing grit size (240, 320, 400 and 600) abrasive papers. To perform fine grinding, samples were manually drawn back to front (one direction only) across the paper. Each step was done for approximately 5 min. After proper washing and drying, grinding with next grid paper was performed. Specimens were rotated 90° after each step. The specimens were thoroughly washed between steps in the polishing process to prevent abrasive particles from being carried to finer grit papers. Fine grinding was performed on the grinder using a continuous water flow for lubrication. Final polishing was done using METADI II Diamond compound (Buehler, Lake Bluff, IL) and a nylon polishing cloth (Buehler, Lake Bluff, IL) on the Buehler grinder/polisher. METADI II diamond abrasive (9 and 0.1 μm) was distributed uniformly over the polishing cloth using the applicator syringes. A liquid extender was then applied to aid in the distribution of diamond particles and to provide lubrication. This step was done for 15–30 min. Samples were unmounted and cleaned with Extran™ detergent and acetone in an ultrasonic cleaner at 60°C in two different steps of 10 min and finally rinsed in double distilled water for 5 min at the final preparation step prior to etching.

2.2 Chemical etching and grain size measurement

Mechanically polished samples were etched using glycergia (3 ml glycerol ($C_3H_5(OH)_3$) + 1 ml HCl + 1 ml HNO_3). Small pool of etchant was created on the sample surface and the samples were cleaned after approximately 30 s in double distilled water. Grain size of the chemically etched samples was measured using American Society for Testing of Materials (ASTM) E112 standard [30]. Following equation was used:

$$n = 2^{G-1} \quad (1)$$

where n stands for the number of grains per square inch at 100× magnification, and G is the ASTM grain size number.

2.3 Contact angle and adhesion energy

Water contact angle measurement (VCA 2500 XE System, Korea) was used to evaluate the hydrophobicity or hydrophilicity of the mechanically polished and chemically etched 316L SS surfaces. The water contact angle of the samples was measured using the sessile drop method. This method is based on axisymmetric drop surface analysis (ASDA) [31]. The angle between the baseline of the drop and the tangent at the drop boundary is measured. Measurements of contact angle were carried out in triplicate. For samples showing varying results, up to five measurements were carried out. The process used for measuring the contact angles was as follows.

The sample was secured in a holder and placed on the VCA stage illuminated for video camera viewing. A stainless steel capillary with a small diameter was used to

administer the double distilled water droplet on to sample surface using a manual thumbscrew control. The same capillary was used for all measurements to ensure no error occurred between measurements. The syringe pump ensured the same size water droplet was delivered to the sample surface each time analysis was carried out. The video camera was attached to a computer, enabling the image of the drop and the samples to be viewed on the computer screen. Thus, it is from this image of the water droplet on the computer screen, that the contact angle was determined. Analysis was carried out using VCA version 1.49 software. At equilibrium the contact angle can be used to determine the interfacial energy. According to the Young-Dupré equation [32]:

$$\gamma(1 + \cos\ \theta) = \Delta W_{SL} \quad (2)$$

where γ is the liquid-vapor surface tension, θ is the contact angle and ΔW_{SL} is the adhesion energy (negative interface free energy) per unit area of the solid and liquid surfaces. γ for water-air is 0.07197 N/m at 25°C [33]. Using Eq. 2 the adhesion energy was calculated.

2.4 Atomic force microscopy

A Veeco Digital Instruments Dimension 3100 atomic force microscope (AFM) was used to measure the surface roughness of the mechanically polished and chemically etched 316L SS samples. A triangular silicon-nitride tip mounted on a cantilever (stiffness constant 0.42 N/m) was operated in contact mode. Each sample was scanned in six different randomly selected locations; the total scan area was $20 \times 20\ \mu m^2$. Root mean square (RMS) roughness (Rq) and average roughness (Ra) values were calculated from $2 \times 2\ \mu m^2$ area within the middle of the scanned area using a Nanoscope IIIa analyzing software. In the case of chemically etched samples, separate roughness values were estimated for the grains and for the grain boundaries.

2.5 X-ray photoelectron spectroscopy

X-ray photoelectron spectroscopy (XPS) was used to analyze the surface chemical composition of mechanically polished and chemically etched 316L SS surfaces. XPS measurements were carried out using a Kratos Axis Ultra spectrometer (Kratos Analytical Inc., GB). A monochromatic X-ray source equipped with an aluminium anode (Al $K\alpha = 1456.6$ eV) operating at 210 W (15 kV, 14 mA) and approximately 3×10^{-7} Pa was used. The emitted photoelectrons were analyzed using a hemispherical energy analyzer, operating in the constant analyzer energy mode. The angle between the plane of the sample and the analyzer lens axis was 90° for all measurements. Survey spectra were taken at analyzer pass energy of 160 eV; high resolution spectra of selected energy intervals at pass energy of 40 eV. XPS spectra show a laterally averaged composition of the analyzed area ($\sim$0.8 mm across). Each sample was analyzed at three different locations. The atomic percentages of the elements present on the analyzed surfaces were calculated using the CasaXPS (version 2.2.68) software and the atomic sensitivity factors included in it.

2.6 Human aortic endothelial cell culture

Prior to incubation with cultured HAECs, mechanically polished and chemically etched samples were cleaned in acetone (15 min) followed by rinsing in double distilled water (10 min) with ultrasonic agitation at 60°C. Samples were then sterilized in a laminar flow culture hood in the presence of a strong UV light for 24 h. HAECs were seeded (2000 cells/ml, 4 ml/sample) on 316L SS samples placed in tissue culture wells for 8 h. Samples were incubated at 37°C and 5% CO_2. HAECs were obtained commercially from Clonetics, Inc. (San Diego, CA) and used between passages 4 and 10. Cells were trypsinized and subcultured in culture medium (MCDB-131; Sigma, St. Louis, MO), supplemented with fibroblast growth factor, epidermal growth factor, hydrocortisone, and penicillin/streptomycin and containing 10% bovine calf iron supplemented serum (Hyclone, OR) at 37°C in a 5% CO_2 incubator. Identity and homogeneity of human aortic endothelial cell cultures were routinely checked by Factor VIII antigen immunofluorescence along with light microscopic inspection of cell morphology and growth patterns. All cell cultures were routinely checked for mycoplasma contamination. After the specified incubation time (8 h), endothelial cells were rinsed with PBS for 1 min followed by fixing with 4% formaldehyde in PBS and again rinsed in PBS. To improve the cell visualization, fixed cells were stained with 2% Giemsa. Cell counting was carried out using a stratified random sampling method. Attached cells were counted on 60 different fields using reflective light microscopy. For calculating the cell spreading area, representative images were captured with the use of a CCD camera coupled to a fluorescence/light microscope (Zeiss Axioplan 2 Imaging, Carl Zeiss Microimaging Inc., NY). Images were then analyzed using NIH Image J 1.62.

Number of activated focal adhesion contacts formed by the cells after 8 h on mechanically polished and chemically etched samples of varying grain sizes were estimated using NIH Image J 1.62 (National Institute of Health, MD). To prepare the cells for evaluation of the number of focal adhesion points, cells were rinsed with PBS and fixed with 4% formaldehyde in PBS followed by rinsing again in PBS. Fixed cells were permeabilized with 0.2% Triton X-100 in PBS for 6 min followed by rinsing briefly 3 times

with PBS and 2 times with 5% BSA in PBS. To indentify active (phosphorylated) focal adhesion sites samples were incubated for 1 h at 37°C in 200 µl of antibody solution (P-FAK-rabbit) diluted in PBS in the ratio 1:100. After 1 h the samples were rinsed 3 times with PBS and 2 times with 5% BSA and dried. 200 µl of Fluorochrome (antirabbit Q DOT 655 goat) diluted (1:200) in PBS was added to the samples and incubated for 1 h at 37°C. Finally, cells were rinsed 3 times with PBS and analyzed using fluorescence microscope and NIH Image J 1.62.

3 Results

3.1 Grain size measurement

Figure 1 shows the results of grain size measurements and calculation using ASTM standard E112. One way ANOVA and Student's *t* test were performed to determine the statistical significance between these sets of samples. It was observed that all the grain sizes (16, 31, 47 and 66 µm) estimated from four different sets of samples were statistically different from each other ($P < 0.001$) and the actual size was not different from the nominal size. Figure 2a–d represents optical micrographs of chemically etched 316L SS samples of 16, 31, 47 and 66 µm grain sizes respectively. The chemical etching of the samples with glycergia resulted in the formation of grain boundary (indicated by arrows in Fig. 2c) orientation dependent surface morphology. The surface topography that forms after the chemical etching of the samples is highly dependent on the material microstructure with protruding grains having a lower dissolution rate as compared to the grain boundaries.

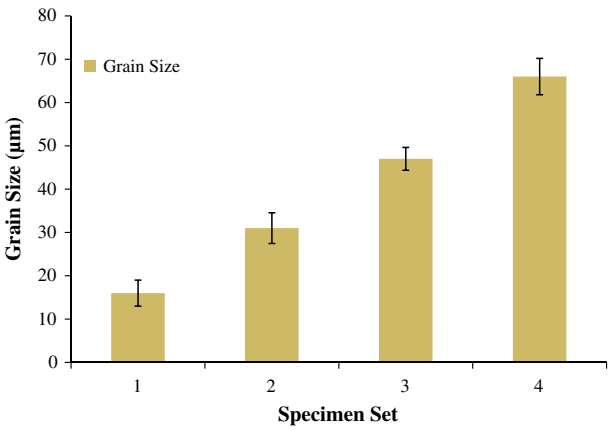

Fig. 1 Bar graph showing grain size values on four different sets of specimens ($n = 15$, $P < 0.001$)

3.2 Contact angle and adhesion energy

Figure 3a, b shows the contact angle and adhesion energy measured on mechanically polished and chemically etched samples as described above. No statistically significant difference in contact angle was observed on mechanically polished samples of different grain sizes. In contrast, chemically etched samples of 16 µm grain size exhibited the lowest contact angle of 40.2 ± 1.7° (highest adhesion energy) whereas the highest contact angle of 86.0 ± 1.1° (lowest adhesion energy) was observed on 66 µm grain size specimens. Contact angle and adhesion energy values for 66 µm mechanically polished and chemically etched specimens showed no statistically significant difference.

3.3 Atomic force microscopy

Average/mean roughness (Ra) values for mechanically polished and chemically etched samples were measured by atomic force microscopy (AFM). Figure 4 shows a comparison of roughness values for mechanically polished sample and chemically etched sample averaged over all grain sizes. Since the chemically etched samples showed different microstructural features, the roughness values were estimated separately on grains and grain boundaries. Roughness of mechanically polished samples was 5.0 ± 0.4 nm and of chemically etched samples were 35.5 ± 2.0 nm (16 µm, ASTM 9), 22.1 ± 4.33 nm (31 µm, ASTM 7), 9.11 ± 0.544 nm (47 µm, ASTM 5.8), 6.28 ± 0.56 nm (66 µm, ASTM 4.9) (Fig. 5). The average roughness (Ra) of chemically etched samples of 16, 31 and 47 µm was significantly higher ($P < 0.01$) as compared to their corresponding mechanically polished samples. Also, a significant difference in roughness values exists between samples of different grain sizes. In summary, the roughness values increased after chemically etching of the samples.

3.4 X-ray photoelectron spectroscopy

X-ray photoelectron spectroscopy (XPS) was done to evaluate the surface chemistry of mechanically polished (MP) and chemically etched (CE) samples (Table 1). Hydrogen is undetectable in XPS and the presence of carbon might be related to surface contamination which occurs due to the fact that the samples are exposed to air before the XPS measurement, hence, these two elements were excluded from the evaluation. The binding energies of Ni 2p peaks indicate that in all the samples nickel is present in the elemental form; all or most of the Ni signal originates from the steel beneath the oxide film. The line shapes of the Fe 2p and Cr 2p signals indicate that these signals originate in part from the metal beneath the oxide film and in part in the oxide film. Atomic concentration of iron was

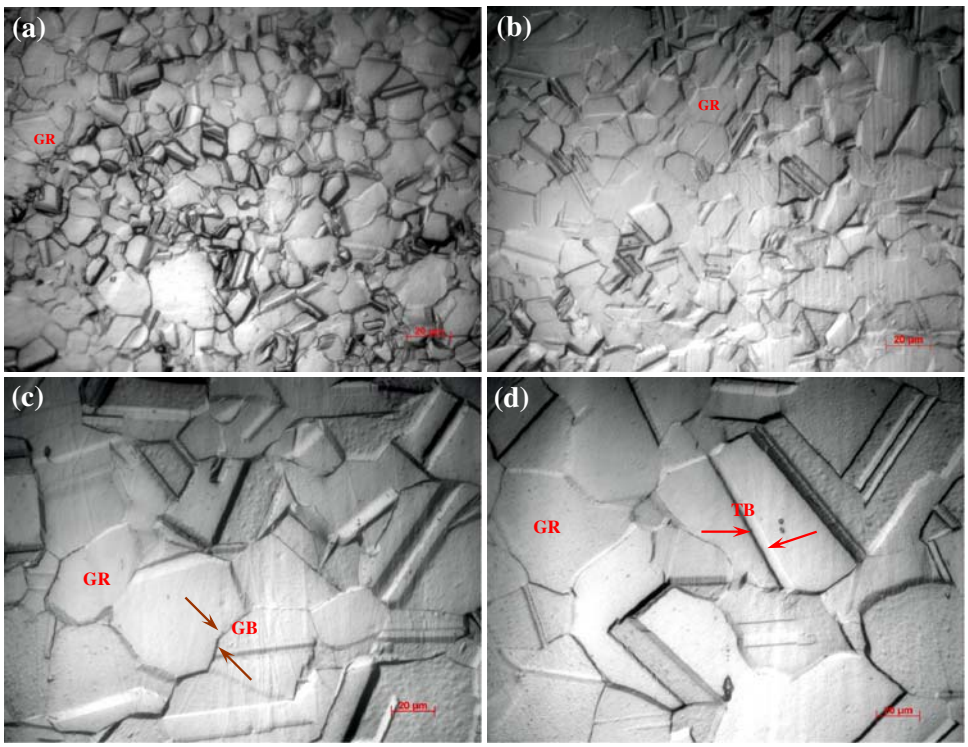

Fig. 2 Optical micrographs of **a** 16 μm, **b** 31 μm, **c** 47 μm, **d** 66 μm 316L SS specimens showing single phase austenitic (γ) microstructure and presence of grains (GR), grain boundaries (*GB* indicated by *arrows*) and twin boundaries (*TB* indicated by *arrows*) (bar = 20 μm)

somewhat higher on MP samples as compared to CE samples and the proportion of elemental Fe was also higher. In MP samples chromium was mostly present as oxide with traces of chromium in elemental form while in CE samples very strong peaks for chromium oxide were observed as compared to elemental chromium peaks which were very weak. Significantly higher concentration of molybdenum was observed on CE samples as compared to MP specimens. CE samples exhibited Mo 3d peaks which indicated the presence on in the elemental and oxidized forms. In contrast, in MP samples molybdenum was present in elemental form only. These observations indicate a thinner oxide on the MP specimens than on the CE specimens.

Atomic concentration of oxygen was slightly higher on MP samples as compared to CE specimens. Presence of metallic oxides with some traces of hydroxides was observed on MP samples. Equally strong peaks for metallic oxides and hydroxides were observed on CE samples. Peaks and their corresponding binding energies in MP samples indicate the presence of nitrogen as NH_3 or as part of an organic matrix. In CE samples nitrogen is present predominantly as nitrides and traces of nitrogen in organic matrix and as nitrates.

3.5 Cell count

Human aortic endothelial cells were seeded on polished and etched samples of varying grain sizes. The density of cells in the culture media was 2000 cells/ml and each sample was incubated in 4 ml of cell suspension. Number of endothelial cells attached per surface area is shown in Fig. 6. One way ANOVA and Student's *t* test were performed to determine the statistical significance of the data. No statistically significant difference in cell density was observed between mechanically polished and chemically etched samples of 47 and 66 μm grain sizes, whereas samples of 16 and 31 μm grain sizes showed statistically significant ($P < 0.01$) difference in number of cells attached on polished and etched specimens. Cell density on 16 μm chemically etched samples was significantly higher ($P < 0.01$) as compared to that on mechanically polished/chemically etched samples of 31, 47 and 66 μm grain sizes. These results show that 16 μm grain size is more favorable for HAEC attachment than the larger grain sizes; in addition, chemical etching positively affected the HAEC attachment on 16 and 31 μm grain size specimens.

3.6 Cell spreading

Endothelial cell spreading area (Fig. 7) was estimated using NIH Image J 1.62 software for mechanically polished and chemically etched samples of different grain sizes. Statistically significant difference in cell spreading area between MP and CE samples was observed for 31 μm ($P < 0.001$), 47 μm ($P < 0.01$) and 66 μm ($P < 0.01$) grain size samples; whereas no significant difference was noted for 16 μm grain size specimens. Maximum HAEC

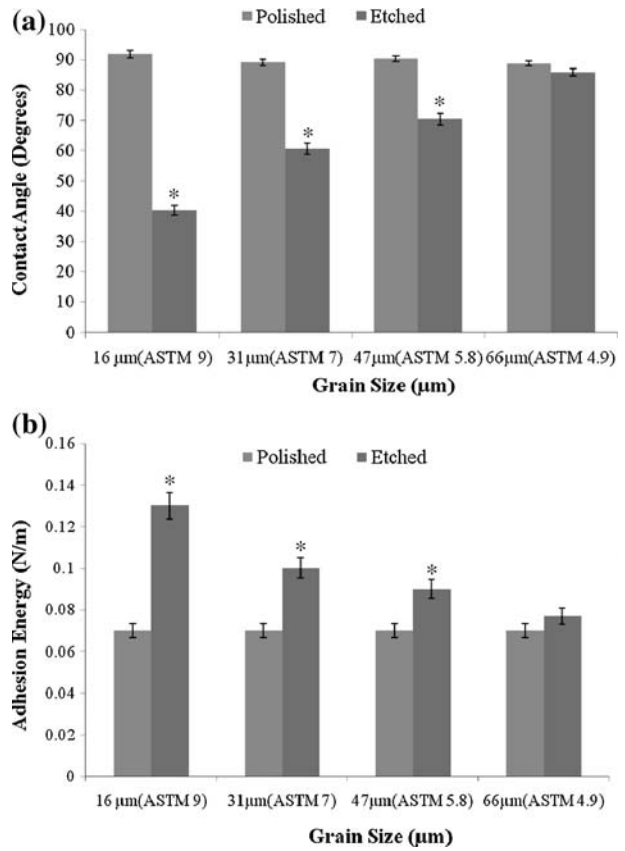

Fig. 3 **a** Contact angle in degrees on mechanically polished and chemically etched 316L SS substrates of varying grain sizes ($n = 20$, * $P < 0.01$). **b** Adhesion energy (N/m) on mechanically polished and chemically etched substrates of varying grain sizes ($n = 20$, * $P < 0.01$)

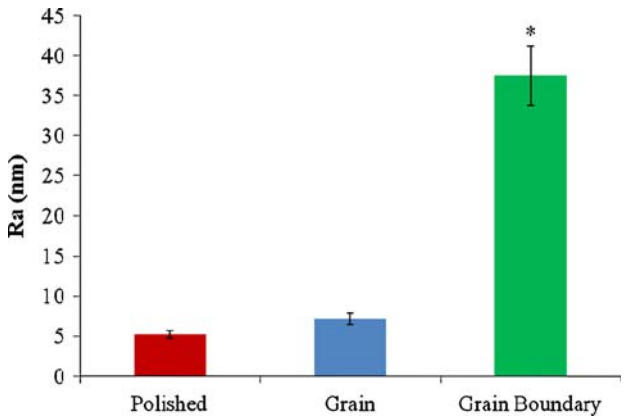

Fig. 4 Average roughness value (Ra) measured on mechanically polished samples and chemically etched (grain/grain boundaries) samples of all grain sizes using atomic force microscope ($n = 40$, * $P < 0.001$)

spreading was observed on 66 µm MP sample (Fig. 8d). It is interesting to note that, HAEC spreading areas on CE specimens of 31, 47 and 66 µm grain sizes are significantly less as compared to the corresponding MP samples, but cell

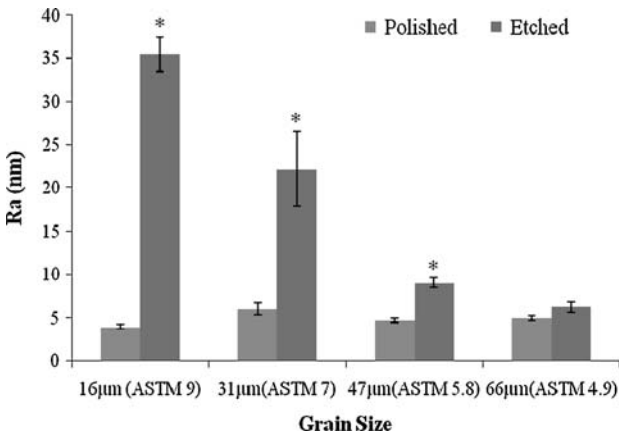

Fig. 5 Average roughness value (Ra) measured on mechanically polished and chemically etched samples of varying grain sizes using atomic force microscope ($n = 10$, * $P < 0.01$)

spreading on 16 µm etched specimen matches up with that of the corresponding polished specimens. Figure 7 also compares the grain areas of 316L SS material microstructure with the endothelial cell spreading areas. Cell spreading areas and grain areas are comparable for chemically etched 47 µm and 66 µm grain size samples, whereas for 16 µm ($P < 0.001$) and 31 µm ($P < 0.01$) grain size samples the difference in significant.

3.7 Morphology of endothelial cells

Endothelial cell morphology on polished and etched samples of different grain sizes is shown in Fig. 8. Bright fluorescence dots in the micrographs represent focal adhesion contacts formed by the cell with the material specimen. Representative micrographs show that the endothelial cell spreading area on CE samples of 31 µm (Fig. 8f), 47 µm (Fig. 8g), and 66 µm (Fig. 8h) is significantly less than that of the corresponding MP samples (Fig. 8b–d). On 16 µm grain size MP and CE samples the endothelial cell spreading areas were comparable (Fig. 8a, e); but on closer observation of the micrographs it is evident that the focal adhesion contacts are more concentrated near the nucleus than at the periphery of the cell in the etched sample (Fig. 8e). In contrast, for polished samples the distribution of focal adhesion contacts appears to be uniform (Fig. 8a). Figure 8d illustrates the largest cell spreading area that was observed on 66 µm grain size samples.

Random endothelial cell shapes were observed on both specimen types of all grain sizes and can be attributed to random shapes of grains in the inherent material microstructure. Figure 9 compares the morphology of endothelial cells on CE 16 and 66 µm grain size samples at 40× magnification. Chemically etched 16 µm samples show

Table 1 Surface chemical composition (at%) measured using X-ray photoelectron spectroscopy (XPS) on mechanically polished and chemically etched 316L SS substrates ($n = 20$)

	Ni (%)	Fe (%)	Cr (%)	O (%)	N (%)	Mo (%)	Cl (%)
MP	0.9 ± 0.3	17.1 ± 3.0	13.0 ± 1.5	64.4 ± 3.5	1.5 ± 0.1	2.2 ± 1.2	0.7 ± 0.3
CE	0.7 ± 0.25	14.0 ± 4.2	16.0 ± 1.6	60.9 ± 3.6	1.9 ± 0.2	3.9 ± 1.1	2.4 ± 1.2

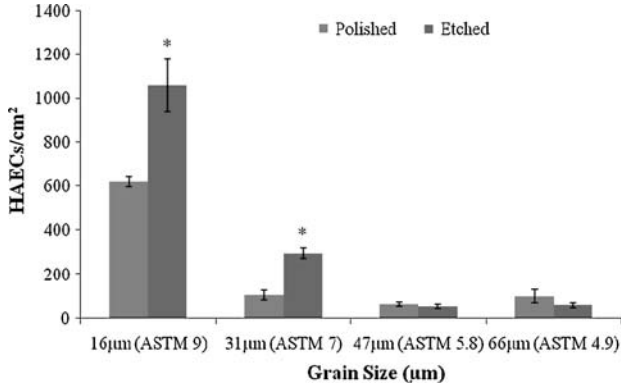

Fig. 6 Bar graph showing the density (cells/cm^2) of endothelial cells attached to mechanically polished and chemically etched 316L SS specimens of different grain sizes ($n = 20$, * $P < 0.01$)

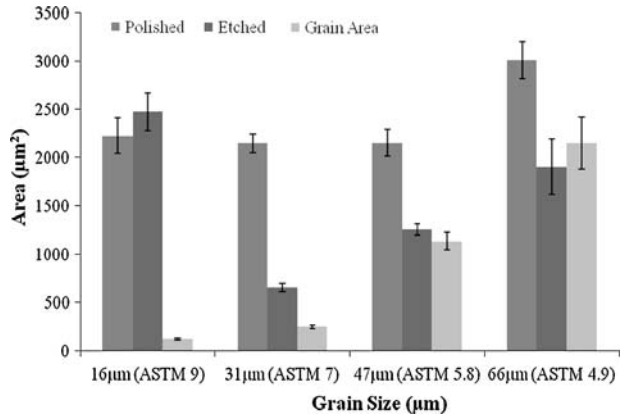

Fig. 7 Bar graph showing the comparison of grain areas (µm^2) and endothelial cell spreading areas (µm^2) on mechanically polished and chemically etched 316L SS specimens of different grain sizes ($n = 10$)

higher cell spreading areas, formation of cell–cell junctions and cell dividing on the surface (Fig. 9a). In contrast, on 66 µm grain size samples rounded HAEC morphology was observed and there was no evidence of cell–cell interaction or extracellular matrix formation (Fig. 9b). Overall, endothelial cells on 16 µm etched surfaces appear to have spread on the grains and bridged across the grain boundaries forming a homogenous covering by cells without any special orientation. In contrast, on other sample types, irregular endothelial cell growth with large uncovered areas and cracks in cell cytoskeleton was observed. No evidence of foreign body giant cells (FBGCs) was observed on any of the samples but relatively more fields on MP and 66 µm grain size CE samples showed signs of dead endothelial cells and debris.

3.8 Focal adhesion contacts

Focal adhesion kinase (FAK) is a non-receptor tyrosine kinase that plays an important role in normal cellular processes such as adhesion, spreading, migration, proliferation and survival. In cultured cells FAK is localized to focal adhesion contacts and becomes phosphorylated and activated in response to integrin-mediated binding of cells to the extracellular matrix, suggesting an important role in cell adhesion and/or migration. Figure 10 shows the number of activated focal adhesion contacts formed by endothelial cells on polished and etched samples of varying grain sizes. Statistically significant differences were observed between MP and CE sample groups of all grain sizes ($P < 0.01$). Maximum number of focal adhesion contacts was observed for 16 µm and minimum for 66 µm grain size samples. Similar trend of decrease in number of focal adhesion contacts from 16 to 66 µm was observed for MP and CE samples.

4 Discussion

The biological performance of biomedical implants strongly depends on the first interaction when implant surfaces come into contact with a biological environment [34]. Healing of biomaterial varies depending on the type and structure of material and the tissue surrounding the implant [34, 35]. Surface characteristics of implants, such as the chemistry, surface charge and the topography of the material surface, influence such interactions and the biological performance of materials [34]. Surface chemistry and topography are broadly recognized as two of the most important factors that influence biological reactions [35]. Surface chemical compositions of biomaterials have a strong influence on the protein adsorption process and are well documented [36–38]. The effects of surface topography on protein adsorption and cell adhesion behavior have been extensively investigated and reported [39–41]. However, since in previous studies topographical variations of

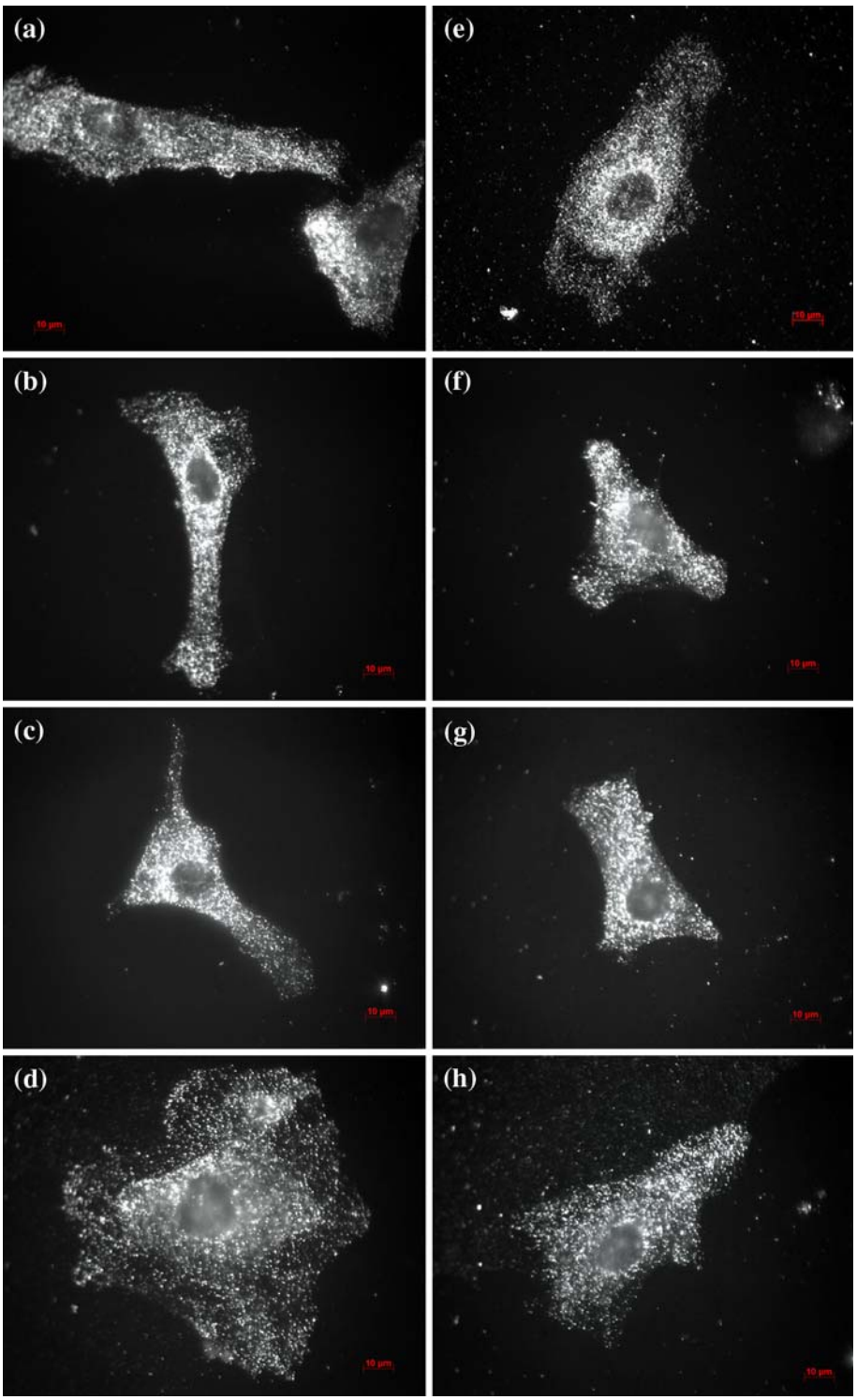

Fig. 8 Morphology of human aortic endothelial cells on 16 μm (**a**, **e**), 31 μm (**b**, **f**), 47 μm (**c**, **g**), 66 μm (**d**, **h**) mechanically polished (**a**, **b**, **c**, **d**) and chemically etched (**e**, **f**, **g**, **h**) 316L SS specimens (mag: 63×, bar: 10 μm)

materials were accompanied by chemical heterogeneities, distinguishing topographical from chemical effects is quite difficult in most cases [42–44].

In this study, we examined the effect of varying 316L SS material microstructure on human aortic endothelial cell attachment and spreading. The results were compared with those obtained on mechanically polished samples with the same grain sizes. The samples were characterized using contact angle, AFM and XPS. Data suggest that 16 μm CE sample showed significantly higher HAEC density and spreading area as compared to CE samples of other grain sizes. The number of focal adhesion sites was also higher on 16 μm grain size specimen as compared to 31, 47 and 66 μm chemically etched samples.

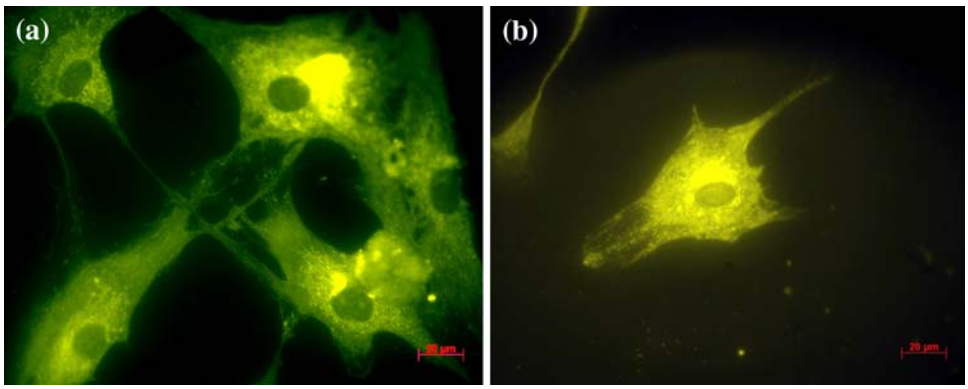

Fig. 9 Fluorescence micrographs (40×) showing morphology of the endothelial cells attached to chemically etched 316L SS specimens of **a** 16 μm and **b** 66 μm grain sizes after 8 h of cell culture

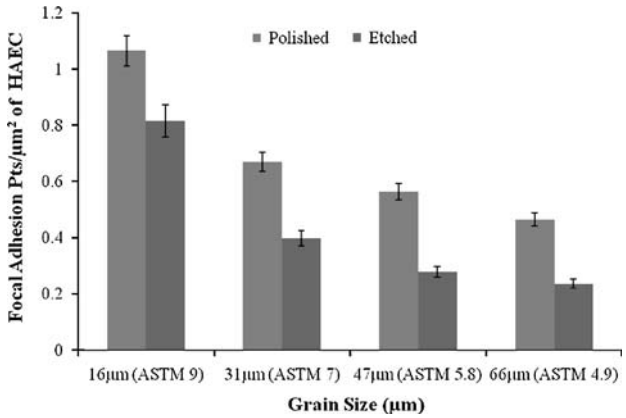

Fig. 10 Bar graph showing the number of activated focal adhesion sites per μm^2 of endothelial cell on mechanically polished and chemically etched 316L SS specimens of different grain sizes ($n = 20$, $P < 0.01$)

In order to better understand the underlying cause of HAECs responding differently to chemically etched samples of different grain sizes, it is important to understand the characteristics and composition of 316L SS, the most commonly used cardiovascular implant material. The "L" in the designation denotes low carbon content (<0.03 wt%), which reduces the possibility of corrosion. The 316L SS alloy is predominantly iron (60–65 wt%) alloyed to major amounts of chromium (17–19 wt%) and nickel (13–15 wt%), plus minor amounts of manganese and molybdenum. There are tight limits for the maximum allowed amounts of phosphorous, sulfur, nitrogen, silicon and copper. The rationale for the alloying additions involves the metals surface and bulk microstructure. 316L SS is covered with a strongly adherent oxide layer that consists mostly of Cr_2O_3 oxide. This oxide layer is different on differently prepared 316L SS. The oxide that is formed during production of 316L sheets is completely removed during mechanical polishing and a native oxide is formed due to exposure to air. In the case of the MP specimens, a thin semi-amorphous, highly damaged layer is beneath this native oxide film. In the process of chemical etching, the damaged layer is removed and grains and grain boundary which differ in chemical composition or charge concentration are exposed [45–47]. A new, thin native oxide is also formed on the surface. According to ASTM F138, F139 specifications, the recommended 316L SS microstructure is single phase austenite (FCC) grains of grain size ASTM 6 or finer, separated by grain boundaries and free from ferritic (BCC) or carbide phases and inclusions such as sulfide stringers [45]. Grain boundary is the dividing surface between two adjacent crystals having different crystallographic orientation. When examined under a microscope after chemical etching grain boundaries in a polycrystalline material like 316L SS, show up as lines and different constituents reflect the light in different ways (Fig. 2). In reality, the grains and grain boundaries are three dimensional; the atoms in the regions of the grain boundary are displaced from their lattice positions to positions of lowest energy due to lattice misfit where the crystals meet. Hence, an increased energy above the normal lattice energy is associated with the displaced atoms at the boundary, giving rise to localized grain boundary energy [48–50].

Findings of this study (Fig. 2) show the expected single phase austenitic (γ) structure. Figure 3 shows the contact angle and adhesion energy on mechanically polished and chemically etched 316L SS samples of different grain sizes. The large differences observed in contact angles (and therefore in surface free energy) are not likely due to surface roughness differences. Surface chemistry or surface charge may cause such effects, but the effect of grain boundaries on contact angle (and adhesion energy) measured on chemically etched specimens is evident. As the grain size decreases, the relative area occupied by the grain boundary increases, therefore, the surface free energy increases and contact angle decreases. Mechanically polished samples showed significantly higher contact angle and greater hydrophobicity as compared to chemically etched samples ($P < 0.01$). Smooth mechanically polished

surfaces where the damaged layer suppresses the microstructural features of the material exhibit lower adhesion energy.

Palmaz et al. [6, 7] have shown that 316L SS specimens with 15 μm grooves exhibited maximum endothelial cell adhesion. The typical size of endothelial cells is 10–20 μm [51], which is comparable to the 16 μm grain size exposed on the chemically etched samples in the current study. As discussed above, small grain size CE samples have higher adhesion energy and greater roughness as compared to higher grain size CE specimens. Hence, a more intense interaction of endothelial cells with the grain boundaries on 16 μm grain size chemically etched samples may explain the increased endothelial cell density and cell spreading on these samples. According to our data, 16 μm grain size specimens seem to have significant impact on initial attachment phase of endothelial cells and subsequent spreading. Endothelial cell behavior on mechanically polished samples and chemically etched samples indicate that initially cells adhered to the surfaces and their distribution was regular but once the cells entered the active adhesion phase they were probing for intercellular and surface contacts. Cells which see limited or no adhesion sites as in case of chemically etched and mechanically polished samples of larger grain sizes can hardly extend anymore to less adhesive surrounding and enter in apoptosis and release apoptosis signal to the surrounding cells. Whereas, on 16 μm grain size 316L SS specimen, cells with good focal adhesion complexes have grown uniformly over the surface and cells are in proliferation phase with some cells migrating towards uncovered surface. Therefore, it can be inferred that grain boundary is acting as a stimulus for cell adhesion and spreading on chemically etched samples. Figure 4 shows that in chemically etched samples the presence of grain boundaries is the main cause of increase in roughness values which might be due to the chemistry or surface charge difference between the grains and grain boundary or simply due to the topography; which will be investigated in future course of the experiments. But it is evident that the presence of more grain boundary area in the 16 and 31 μm chemically etched samples appears to be the major cause of large increase in roughness value because lower roughness values were measured on 66 μm grain size samples, which have comparatively less grain boundary area.

The role of surface chemistry of 316L SS material specimens (polished and etched) in mediating human aortic endothelial cell response is rather unclear. The toxic effects of nickel have been linked to increased levels of oxidative stress found within endothelial cells exposed to nickel ions. The permeability of the endothelium increases and its barrier function impaired by generation of intracellular oxygen radicals e.g. OH. Surface nickel species therefore influence the biocompatibility of the alloy. The literature reports that the predominant effect of nickel on the endothelial cells is on the expression of VE-cadherin and F-actin within endothelial cells grown to confluence following the 72 h of culture on NiTi alloy [52]. Results of the current experiment reveal no significant amount of Ni on the specimen surfaces and no significant differences between mechanically polished and chemically etched samples. Thus nickel is not likely to affect the results. Similarly, other elements like iron (difference $\sim$3.16%) and molybdenum (difference $\sim$1.74%) showed no significant difference on the samples to cause a significant difference in the HAEC behavior as observed in current study. In contrast, the chromium, exhibited significant difference ($\sim$3.05%). The higher chromium content of the oxide might enhance HAEC attachment and spreading on the surface of chemically etched samples. However, it is more likely that interaction of endothelial cells with material microstructure has a major effect. A more detailed analysis of any difference in chemistry of grains and grain boundary is needed which is beyond the scope of this study.

5 Conclusion

Grain boundary etched 316L SS material of varying grain sizes in attachment and spreading of endothelial cells was investigated. Results indicate the potential of 16 μm chemically etched sample in increasing the rate of endothelialization. The findings of this study suggest that increasing the grain boundary area increases the adhesion energy of the substrate and enhances the endothelial cell density (more for 16 μm as compared to 66 μm grain size samples) on the surface. When compared with smooth mechanically polished samples, 16 μm chemically etched samples exhibited higher endothelial cell density.

Acknowledgement The authors thank Aaron Watson, Jian Luo and Lee Cardenas for their expert technical assistance.

References

1. Whittaker DR, Fillinger MF. The engineering of endovascular stent technology: a review. Vasc Endovascular Surg. 2006;40(2): 85–94. doi:10.1177/153857440604000201.
2. Schatz RA, Palmaz JC, Tio FO, Garcia F, Garcia O, Reuter SR. Balloon-expandable intracoronary stents in the adult dog. Circulation. 1987;76:450–7.
3. Palmaz JC, Tio FO, Schatz RA, Alvardo R, Rees C, Garcia O. Early endothelialization of balloon-expandable stents: experimental observations. J Vasc Interv Radiol. 1988;3:119–24.
4. Palmaz JC. Intravascular stents: tissue-stent interactions and design considerations. AJR. 1993;160:613–8.

5. Simon C, Palmaz JC, Sprague EA. Influence of topography on endothelialization of stents: clues for new designs. J Long Term Eff Med Implants. 2000;10:143–51.
6. Palmaz JC, Benson A, Sprague EA. Influence of surface topography on endothelialization of intravascular metallic material. J Vasc Interv Radiol. 1999;10:439–44. doi:10.1016/S1051-0443(99)70063-1.
7. Fuss C, Sprague EA, Bailey SR, Palmaz JC. Surface micro grooves (MG) improve endothelialization rate in vitro and in vivo. Am J Cardiol. 2001;37(2A):70A.
8. Hamuro M, Palmaz JC, Sprague EA, Fuss C, Luo J. Influence of stent edge angle on endothelialization in an in vitro model. J Vasc Interv Radiol. 2001;12:607–11. doi:10.1016/S1051-0443(07)61484-5.
9. Van Belle E, Tio FO, Couffinhal T, Maillard L, Passeri J, Isner JM. Stent endothelialization: time course, impact of local catheter delivery, feasibility of recombinant protein administration, and response to cytokine expedition. Circulation. 1997;95:438–48.
10. Van Belle E, Tio FO, Chen D, Maillard L, Kearney M, Isner JM. Passivation of metallic stents following arterial gene transfer of phVEGF165 inhibits thrombus formation and intimal thickening. J Am Coll Cardiol. 1997;29:1371–9. doi:10.1016/S0735-1097(97)00049-1.
11. Costa MA, Sabat M, van der Giessen WJ, Kay IP, Cervinka P, Ligthart JM, et al. Late coronary occlusion after intracoronary brachytherapy. Circulation. 1999;100:789–92.
12. Liistro F, Colombo A. Late acute thrombosis after paclitaxel eluting stent implantation. Heart. 2001;86:262–4. doi:10.1136/heart.86.3.262.
13. Dibra A, Kastrati A, Mehilli J, Pache J, Oepen R, Dirschinger J, et al. Influence of stent surface topography on the outcomes of patients undergoing coronary stenting: a randomized double-blind controlled trial. Catheter Cardiovasc Interv. 2005;65:374–80. doi:10.1002/ccd.20400.
14. Wen X, Wang X, Zhang N. Microrough surface of metallic biomaterials: a literature review. Biomed Mater Eng. 1996;6:173–89.
15. Seliger C, Schwennicke K, Schaffer C. Influence of a rough, ceramic-like stent surface made of iridium oxide on neointimal structure and thickening. Eur Heart J. 2000;21(Suppl):286.
16. Xiao L, Shi D. Role of precoating in artificial vessel endothelialization. Chin J Traumatol. 2004;7:312–6.
17. Rotmans JI, Heyligers JM, Verhagen HJ, Velema E, Nagtegaal MM, de Kleijn DP, et al. In vivo cell seeding with anti-CD34 antibodies successfully accelerates endothelialization but stimulates intimal hyperplasia in porcine arteriovenous expanded polytetrafluoroethylene grafts. Circulation. 2005;112:12–8. doi:10.1161/CIRCULATIONAHA.104.504407.
18. Pislaru SV, Harbuzariu A, Agarwal G, Witt T, Gulati R, Sandhu NP, et al. Magnetic forces enable rapid endothelialization of synthetic vascular grafts. Circulation. 2006;114(1):I314–1318. doi:10.1161/CIRCULATIONAHA.105.001446.
19. Chen CS, Mrksich M, Huang S, Whitesides GM, Ingber DE. Using self-assembled monolayers to control cell shape, position, and function. Biotechnol Prog. 1998;14:356–63. doi:10.1021/bp980031m.
20. Sandrucci MA, Nicolin V, Biasotto M, Breschi L, Casagrande L, Lenarda RD, et al. Adhesion of Flow 2002 fibroblasts to titanium implant materials is influenced by different surface topographies and is related to the immunocytochemical expression of fibronectin. J Appl Biomater Biomech. 2004;2:169–76.
21. Meredith DO, Eschbach L, Riehle MO, Curtis ASG, Richards RG. Human fibroblast proliferation and cytoskeleton reactivity to characterized metal implant surfaces. Eur Cell Mater. 2004;7(1):66.
22. Buehler M, Harris L, Zinger O, Landolt D, Richards RG. Characterization of fibroblast adhesion on titanium model surfaces. Eur Cell Mater. 2003;5(1):24–5.
23. Flemming RG, Murphy CJ, Abrams GA, Goodman SL, Nealey PF. Effects of synthetic micro- and nano-structured surfaces on cell behavior. Biomaterials. 1999;20:573–88. doi:10.1016/S0142-9612(98)00209-9.
24. Falconneta D, Csucsb G, Grandina HM, Textora M. Surface engineering approaches to micropattern surfaces for cell-based assays. Biomaterials. 2006;27:3044–63. doi:10.1016/j.biomaterials.2005.12.024.
25. Kasemo B, Gold J. Implant surfaces and interface processes. Adv Dent Res. 1999;13:8–20. doi:10.1177/08959374990130011901.
26. Webster TJ, Ejiofor JU. Increased osteoblast adhesion on nanophase metals: Ti, Ti_6Al_4V, and CoCrMo. Biomaterials. 2004;25:4731–9. doi:10.1016/j.biomaterials.2003.12.002.
27. Cai K, Bossert J, Jandt KD. Does the nanometre scale topography of titanium influence protein adsorption and cell proliferation? Biomaterials. 2006;49:136–44.
28. Webster TJ, Siegel RW, Bizios R. Osteoblast adhesion on nanophase ceramics. Biomaterials. 1999;20:1221–7. doi:10.1016/S0142-9612(99)00020-4.
29. Standard practice for preparation of metallographic specimens. ASTM E3-95. ASTM International; 1995. p. 12.
30. Standard test methods for determining average grain size. ASTM E112-96, ASTM International; 2004. p. e2.
31. del Ro OI, Kwok DY, Wu R, Alvarez JM, Neumann AW. Contact angle measurements by axisymmetric drop shape analysis and an automated polynomial fit program. Colloids Surf A Physicochem Eng Asp. 1998;143(2):197–210. doi:10.1016/S0927-7757(98)00257-X.
32. Chow TS. Wetting of rough surfaces. J Phys Condens Matter. 1998;10(27):L445–51. doi:10.1088/0953-8984/10/27/001.
33. Anderson HL. A physicist desk reference. New York: American Institute of Physics; 1989. p. 42.
34. Caster DG, Ratner BD. Biomedical surface science: foundations to frontiers. Surf Sci. 2002;500:28–60. doi:10.1016/S0039-6028(01)01587-4.
35. Galli C, Coen MC, Hauert R, Katanaev VL. Creation of nanostructures to study the topographical dependency of protein adsorption. Colloids Surf B Biointerfaces. 2002;26:255–67. doi:10.1016/S0927-7765(02)00015-2.
36. Sigal GB, Mrksich M, Whitesides GM. The effect of surface wettability on the adsorption of proteins and detergents. J Am Chem Soc. 1998;120:3464–73. doi:10.1021/ja970819l.
37. Kidoaki S, Matsuda T. Adhesion forces of the blood plasma proteins on self-assembled monolayer surfaces of alkanethiolates with different functional groups measured by an atomic force microscope. Langmuir. 1999;15:7639–46. doi:10.1021/la990357k.
38. MaClary KB, Ugarova T, Grainger DW. Modulating fibroblast adhesion, spreading, and proliferation using self-assembled monolayer films of alkyl thiolates on gold. J Biomed Mater Res A 50:428–439. doi:10.1002/(SICI)1097-4636(20000605)50:3<428::AID-JBM18>3.0.CO;2-H.
39. Wojciak BS, Curtis A, Monhagan W, Macdonald K, Wilkinson C. Guidance and activation of murine macrophages by nanometric scale topography. Exp Cell Res. 1996;223:426–435. doi:10.1006/excr.1996.0098.
40. Wei S, Hong C. Protein adsorption on materials surfaces with nano-topography. Chin Sci Bull. 2007;52(23):3169–3173. doi:10.1007/s11434-007-0504-6.
41. Dufrene YD, Marchat TG, Rouxhet PG. Influence of substratum surface properties on the organization of adsorbed collagen films: in situ characterization by atomic force microscopy. Langmuir. 1999;15:2871–8. doi:10.1021/la981066z.

42. Curtis A, Wilkinson C. Topographical control of cells. Biomaterials. 1998;18:1573–83. doi:10.1016/S0142-9612(97)00144-0.
43. Diener A, Nebe B, Lüthen F, Becker P, Beck U, Neumann NG, et al. Control of focal adhesion dynamics by material surface characteristics. Biomaterials. 2005;26(4):383–92. doi:10.1016/j.biomaterials.2004.02.038.
44. Rocha LB, Goissis G, Rossia MA. Biocompatibility of anionic collagen matrix as scaffold for bone healing. Biomaterials. 2002;23(2):449–56. doi:10.1016/S0142-9612(01)00126-0.
45. Brunski JB. Metals. In: Ratner BD, Hoffman AS, Schoen FJ, Lemons JE, editors. Biomaterials science an introduction to materials in medicine. 2nd ed. San Diego: Elsevier Academic Press; 2004. p. 137–153.
46. Chadwick GA. Grain shapes and phase distribution. In: Metallography of phase transformations. New York: Butterworth and Co. Publisher; 1972. p. 160–182.
47. Alexander WO, Davis S, Heslop S, Reynolds KA, Whittaker VN. The origins of the strength of metals. In: Bradbury EJ, editor. Essential metallurgy for engineers. Berkshire: Thetford Press Ltd; 1985, p. 33–79.
48. Sutton AP, Balluffi RW. Overview no. 61: on geometric criteria for low interfacial energy. Acta Metall. 1987;35(9):2177–201. doi:10.1016/0001-6160(87)90067-8.
49. Doherty RD, Hughes DA, Humphreys FJ, Jonas JJ, Juul Jenson D, Kassner ME, et al. Current issues in recrystallization: a review. Mater Sci Eng A. 1997;238:219–74. doi:10.1016/S0921-5093(97)00424-3.
50. Mishra S, Narasimhan K, Samajdar I. Deformation twinning in AISI 316L austenitic stainless steel—role of strain and strain path. Mater Sci Technol. 2007;23(9):1118–26. doi:10.1179/174328407X213242.
51. McGeachie J. Blue histology—vascular system. The School of Anatomy and Human Biology, The University of Western Australia. http://www.lab.anhb.uwa.edu.au/mb140/MoreAbout/Endothel.htm. Accessed 2nd February 2008.
52. Plant SD, Grant DM, Leach L. Behaviour of human endothelial cells on surface modified NiTi alloy. Biomaterials. 2005;26:5359–67. doi:10.1016/j.biomaterials.2005.01.067.